FSI-analysis of a Francis turbine

Jonas Bergmann-Paulsen

NTNU
Norwegian University
of Science and Technology

Department of Energy
and Process Engineering

EPT-M-2012-18

MASTER THESIS
for
Jonas Bergmann-Paulsen
Spring 2012

FSI-analysis of a Francis turbine
FSI-analyse av en Francis turbin

Background

Sediment erosion in Francis turbines is a large problem for river power plants near the Himalayas and the Andes Mountains. Due to high sediment concentration in the rivers the turbine components are exposed to erosion wear and must be maintained often. During monsoon periods, the sediment concentration is at its highest and the turbines are stopped to reduce the damage on the components. The turbines at Jhimruk Power Plant in Nepal are a good example on how the sediment erosion effects the power plant operation. These turbines need to be maintained annually due to high erosion wear. This result in a reduction of power production and high maintenance cost. It is therefore of interest to design a new Francis turbine which is more resistant to sediment erosion. A cooperation between Kathmandu University and NTNU has started and aim to start manufacture Francis turbines that can withstand high sediment load.

The new turbine design will require analysis of both hydraulic efficiency and material strength. The material strength is affected by the hydraulic loads of the turbine and it will be evaluated by using tools to analyze the fluid-structure interaction, FSI.

Objective:
FSI-analysis of a Francis turbine

The following tasks are to be considered:

1. Literature survey
   a. Mechanical design of Francis turbines
   b. FSI-analysis of Francis turbines

2. Software knowledge
   a. Get familiar with the CFD-tool; Ansys
   b. Get familiar with the FSI-tool; Ansys

3. The student will carry out FSI-analysis of a Francis turbine. This will be carried out on selected components which will be decided during the design study.

4. If there are time available, a complete 3D-CAD model will be developed
   a. During the student's project work in the fall semester, a 3D-CAD model has been drawn in the CAD-tool Pro-Engineer. This work will be further developed in order to have a complete model of the Francis turbine that is analyzed in this master project.

Within 14 days of receiving the written text on the master thesis, the candidate shall submit a research plan for his project to the department.

When the thesis is evaluated, emphasis is put on processing of the results, and that they are presented in tabular and/or graphic form in a clear manner, and that they are analyzed carefully.

The thesis should be formulated as a research report with summary both in English and Norwegian, conclusion, literature references, table of contents etc. During the preparation of the text, the candidate should make an effort to produce a well-structured and easily readable report. In order to ease the evaluation of the thesis, it is important that the cross-references are correct. In the making of the report, strong emphasis should be placed on both a thorough discussion of the results and an orderly presentation.
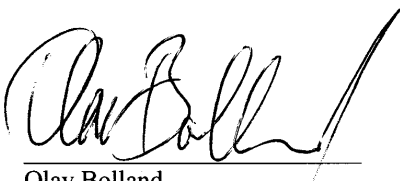
The candidate is requested to initiate and keep close contact with his/her academic supervisor(s) throughout the working period. The candidate must follow the rules and regulations of NTNU as well as passive directions given by the Department of Energy and Process Engineering.

Risk assessment of the candidate's work shall be carried out according to the department's procedures. The risk assessment must be documented and included as part of the final report. Events related to the candidate's work adversely affecting the health, safety or security, must be documented and included as part of the final report.
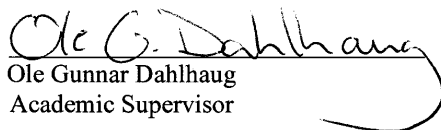
Pursuant to "Regulations concerning the supplementary provisions to the technology study program/Master of Science" at NTNU §20, the Department reserves the permission to utilize all the results and data for teaching and research purposes as well as in future publications.

The final report is to be submitted digitally in DAIM. An executive summary of the thesis including title, student's name, supervisor's name, year, department name, and NTNU's logo and name, shall be submitted to the department as a separate pdf file. Based on an agreement with the supervisor, the final report and other material and documents may be given to the supervisor in digital format.

Department of Energy and Process Engineering, 10. January 2012

Olav Bolland
Department Head

Ole Gunnar Dahlhaug
Academic Supervisor

Research Advisors: Mette Eltvik, PhD-student

Preface

This thesis was written at the Waterpower Laboratory, Department of Energy and Process Engineering at the Norwegian University of Science and Technology (NTNU) during the spring semester 2012. During this thesis I got to visit Kathmandu University (KU) to take part in the cooperation between our universities.

I would like to thank my supervisor Ole Gunnar Dahlhaug for giving me great support, motivating me and giving me the opportunity to travel to Nepal and see what I am actually working on. My co-supervisor Mette Eltvik deserves the same thanks for all the help she has given me and facilitating my stay in Nepal.

I would like to thank everyone at the Turbine Testing Lab (TTL) at KU for making my stay in Nepal great and memorable, I am sure I will come back to visit you soon.

I would like to thank my girlfriend Ida for support and motivation through my studies.

Last but not least I would like to thank everyone at the Waterpower Laboratory, employees and students alike. Thank you for always trying (and succeeding) to make things just a little bit better. Our trip to Nepal is one for the books. I hope we will all meet both at work and after work in the time to come.

Abstract

Sediment erosion in Francis turbines is a big problem in hydropower plants in and around the Himalayas. The sediment composition in the rivers contains high levels of the hard mineral quarts. When the sediments enter the turbine they cause erosive damage to exposed parts such as covers, guide vanes and runner. The sediment concentration is at its highest during the monsoon period. During this period some turbines are stopped when the sediment consentration reaches certain levels to reduce the damage.

Jhimruk power plant in the mid-western part of Nepal is a good example of how the sediment erosion affects the operation of a power plant. During the monsoon period the turbines can be eroded to an almost unrepairable state. The turbines have to go through substantial annually maintenance. A result of this is reduced power output and high maintenance costs. It is therefore of interest to design a new Francis turbine that can better withstand the sediment erosion. A cooperation project between Kathmandu University and The Norwegian University of Science and Technology was started as a part of the RenewableNepal project which aims to develop and start manufacturing of erosion resistant Francis turbines.

A parameter study of different blade designs have been performed to find a more erosion resistant design. In this thesis FSI analyses have been performed on three different designs to verify their structural integrity. The designs transfers the hydraulic energy from the water to the blade in different sections. The results showed a stress distribution which coincided with the energy transfer along the blade. The reference design was analyzed with two different blade thickness. For all the designs the stress was relatively low compared to the criteria for hydraulic turbines.

Sammendrag

Sedimenterosjon i Francisturbiner er et stort problem for vannkraftverk i området i og rundt Himalaya. Elvene i dette området inneholder store mengder sedimenter. Sammensetningen av sedimenter består blant annet det svært harde mineralet kvarts. Vannet renner igjennom turbinene og de harde sedimentene forårsaker store skader på det mekaniske utstyret. Sedimentkonsentrasjonen er på sitt høyeste i monsunperioden, og turbiner må tidvis stenges for å redusere slitasjen.

I den vestlige delen av Nepal ligger Jhimruk vannkraftverk. Jhimruk er et eksempel på hvordan driften av et vannkraftverk i stor grad påvirkes av sedimenterosjon. I løpet av monsunperioden kan turbindelene slites til et nivå der de ikke lengre kan repareres. Det må gjennomføres betydelig vedlikehold hvert år, noe som fører til tapt produksjon og store vedlikeholdskostnader. Det er derfor av stor interesse å designe en Francisturbin som er bedre egnet for drift i områder med mye sedimenter.

Det har tidligere blitt utført et parameterstudie på løpehjulskovldesign med mål om å finne et mer erosjonsmotstandsdyktig design. Studiet viste at ved å endre området energioverføringen fra vannet tar sted på skovlen påvirket erosjonen. I denne oppgaven har det blitt gjennomført FSI-analyser på tre ulike design der et av designene har blitt testet med ulik blad tykkelse. Spenningsfordelingen som ble funnet stemte med antagelsene angående hvor momentet ble overført fra vannet. Alle designene hadde spenninger under kriteriet for hydraulisk maskineri.

Contents

List of Figures

List of Tables

Nomeclature

Abrevations

ATM	Automated Topology and Mesh
CAD	Computer Aided Design
CFD	Computational Fluid Dynamics
FEM	Finite Element Method
FSI	Fluid Structure Interaction
HB	Brinell hardness
KU	Kathmandu University
NORAD	Norwegian Agency for Development Cooperation
NTNU	Norwegian University of Science and Technology
SST	Shear Stress Transport

Symbols

Symbol	Description	Unit
a	Number of cyclic elements	-
b	Face tolerance angle / height of runner inlet	[-/m]
c_u	Tangential absolute velocity	[m/s]
d	Derivative	-
g	Acceleration of gravity	$[m/s^2]$
h	Head	[m]
h_i	Head at inlet	[m]
h_p	Head at smallest diameter of pump plate	[m]
k	Ratio between c_u and the periphery velocity	-
M	Moment	[Nm]
P	Power	[W]
q	Load	[N/m]
r	Radius	[m]
r_p	Smallest radius of pump plate	[m]
R_1	Biggest radius for moment transfer	[m]
R_M	Moment arm	[m]
R_T	Smallest radius for moment transfer	[m]
t	Blade thickness	[m]
u_τ	Friction velocity	$[m/s]$
V_r	Radial velocity component	-
V_t	Tangential velocity component	-
y	Wall distance	[m]
y^+	Dimensionless wall distance	[-]
ν	Kinematic viscosity	$[m^2/s]$
∂	Partial derivative	-
ρ	Density of water	$[kg/m^3]$
σ	Stress	[Pa]
τ_w	Wall stress	[Pa]
ω	Angular velocity	$[s^{-1}]$

Chapter 1

Introduction

1.1   Background

1.1.1   Hydropower in Nepal

Nepal is placed in the Himalayas which consists of several of the worlds highest mountains. Snow and glaciers cover large areas of the high regions in the country. From June to September the monsoon wind comes from south east and is pushed into the mountains resulting in great amounts of rain. During the monsoon the amount of water is in some rivers increased by between 400 and 1000 times [1].

The total potential of hydropower in Nepal is estimated to be more than 83 000 MW where 43 000 MW is considered economically feasible [1], however in 2011 only 610 MW was utilized [2]. The combination of extreme weather, glaciers and rock with low abrasion resistance produces a periodically very high sediment concentration in the Nepali rivers. The sediments cause problems in the mechanical hydro power equipment as the hard fragments of rock hits the metal and causes severe erosion. In dammed plants the sediments settle in the dam and causes big losses in the storage capacity.

RenewableNepal

The energy demand in Nepal is growing fast and in 2010 the Nepalese government announced its intentions of expanding the hydropower capacity by 38 000 MW the next 25 years [2]. Norway have more than a century of experience with research and development of hydropower, but little knowledge about the problems connected to sediment erosion. The run of river plants in Nepal is exposed to extreme amounts of sediments during the monsoon periods and turbines can be eroded to an unrepairable state during only a short period if they are not shut down. In the light of this it is obvious that new technology has to be developed if the hydro power potential in Nepal is to be utilized. The cost of transporting a turbine is high and it is fair to assume that a local manufacturer could decrease the total cost of a new turbine significantly.

The Norwegian Agency for Development Cooperation (NORAD) supported program RenewableNepal was started to increase the Nepalese competence in hydropower. The short term goal is to develop a center of excellence for research and development of hydraulic turbines at the Kathmandu University. Here the competence and "know how" developed at NTNU over several decades will be transferred to Kathmandu University. The long term goal is to create a turbine manufacturer, here project participants from the Nepalese and Norwegian industry will take a leading role [2].

1.1.2 Jhimruk hydropower plant

Jhimruk hydropower plant is a 12 MW run-of-river plant located in the Mid-Western part of Nepal. The power plant consist of three horizontal axis Francis turbines, each with an capacity of 4,2 MW [3]. 83 percent of the annual rainfall in the area occurs during the monsoon period [3]. The monsoon rain brings high amounts of sediments to the river. The sediment composition contains large amounts of quarts which have a hardness of 7 on the Mohs scale and is considered a very hard mineral [4]. The sand laden water exposes the turbines to severe sediment erosion. Due to this the turbines require considerable annual maintenance. Jhimruk power plant depends on having two sets of turbines for each unit so one set can be repaired while the other set runs.

Table 1.1.1: Data for Jhimruk power plant [3].

Head(m)	201,5
Flow rate(m^3/s)	2,35
Rotational speed(rpm)	1000
Number of blades	17
Speed number	0.3220
Diameter inlet/outlet(m)	0.890/0.540

1.1.3 Earlier and ongoing work

Mechanical design of a Francis turbine exposed to sediment erosion

During the authors project thesis, *Mechanical design of Francis turbine exposed to sediment erosion* [5], a Computer Aided Design (CAD) model of a new turbine for Jhimruk power plant was modelled. The design differs from normal Francis turbine designs in the following areas:

- The turbine is dismantled by removing the draft tube and lower cover first to reduce downtime during maintenance.

- The surfaces of the covers exposed to erosion is protected by coated plates that easily can be exchanged.

- The labyrinth seals are made detachable to ease maintenance or replacement.

Static structural analyses was performed on a guide vane and the covers.

Figure 1.1.1 shows the Francis turbine design from [5].
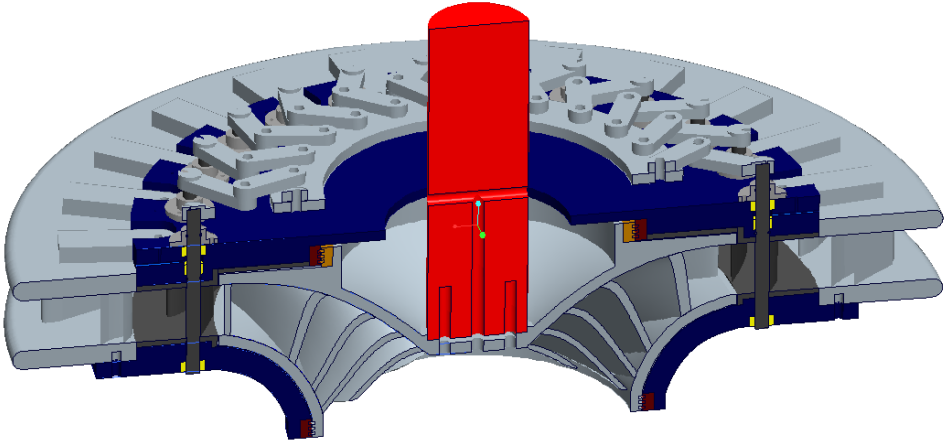
Figure 1.1.1: Francis turbine design for Jhimruk power plant.

Parameter study of Francis turbine blade

The blade angle affects how the hydraulic energy is converted to mechanical energy along the blade [3]. In the paper *Numerical analysis on effect of design parameter and sediment erosion on a Francis runner* by Eltvik [3], the relation between design parameters and its effect on erosion wear on the runner blade was investigated. Figure 1.1.2 shows five blade angle shapes that was investigated.
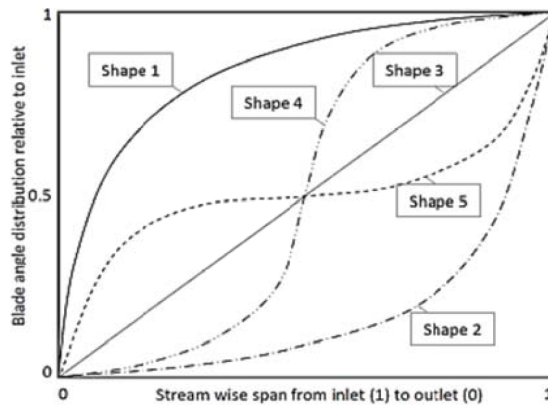
Figure 1.1.2: Blade angle shapes in a Francis runner blade [3].

Shape 1 will convert most of the hydraulic energy from the middle of the blade to the outlet. Shape 2 will convert most of the energy from the inlet to the middle of the blade. A linear blade distribution, shown by shape 3, was chosen as a reference

design [3]. The study showed that a blade with shape 4 will have a reduction of erosion by 60% at the cost of the turbine efficiency. Shape 5 showed a reduction in erosion by 20% at no cost in efficiency [3].

Other similar work

A Fluid structure interaction (FSI) analysis of the runners at the power plant Cahua in Peru were performed in Ola Gjølme Thorvaldsens master thesis *Strength calculations of runners in Francis turbines* [6]. During Helene Palmgren Erichsens master thesis *Mechanical design of a Francis turbine exposed to sediment erosion* [7] an FSI analysis of a blade for the Jhimruk Power plant was performed. Several thesis regarding Computational Fluid Dynamics (CFD) analyses on Francis turbines have been written at the Waterpower laboratory at NTNU. A program for hydraulic design of Francis turbines, *Khoj* has been developed by Gjøsæter [8] and Gogstad [9]. Gogstad and the author made several changes to the program during the authors project thesis [5] to simplify the process of matching *Khoj* and the CAD program*Pro/Engineer*.

PhD Mette Eltvik is currently working on the hydraulic design for Jhimruk Hydro Power plant.

1.1.4 Objective

The objective of this thesis is to verify the structural integrity of three blade designs from the parameter study in +it Eltvik 2012 [3].

Shape 1 and 2 from Figure 1.1.2 represents the extremes in the parameter study. It was therefore decided that Shape 1 (S1), Shape 2 (S2) and Shape 3 (reference design) from [3] would be analysed.

1.2   Francis turbine design

The Francis turbine is a medium to high head turbine that usually operates at heads between 60 and 650 meters [10]. The Francis turbine is a reaction turbine meaning that the energy from both velocity and pressure in the water is converted to mechanical energy by the runner. The reaction turbines are also characterized by the fact that during operation all the channels are filled with water. In comparison an impulse turbine, also called a free jet turbine, converts all the pressure energy in the water to kinetic energy before it enters the runner.

1.2.1   Mode of operation

Water flows from the penstock into the spiral casing. In the spiral casing the water is distributed around the complete periphery. The water is then guided by the stay vanes and guide vanes in the correct angle towards the runner. The guide vanes are adjustable and can change the angle depending on the inlet and outlet conditions of the turbine, they are controlled by a governor servo motor. The runner transfers the energy from the pressure and velocity in the water to a rotational momentum. The water exits through a draft tube that extracts the remaining energy in the water. The torque produced in the runner is transferred to a power producing generator through a shaft [11]. Figure 1.2.1 shows how the potential energy is transformed to kinetic energy towards the runner, and how both kinetic and potential energy is absorbed through the runner.
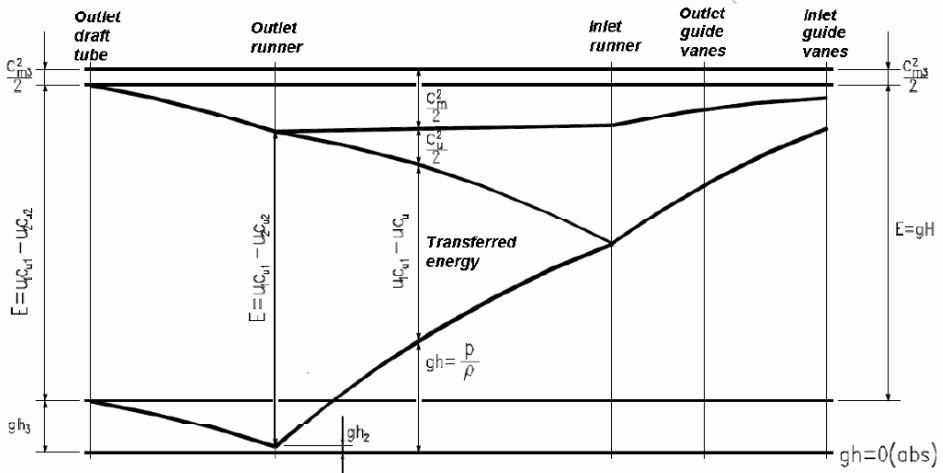
Figure 1.2.1: Energy conversion through a Francis turbine [12].

1.2.2   Main components

Figure 1.2.2 shows a cross section of a vertical axis Francis turbine with the components marked with numbers.
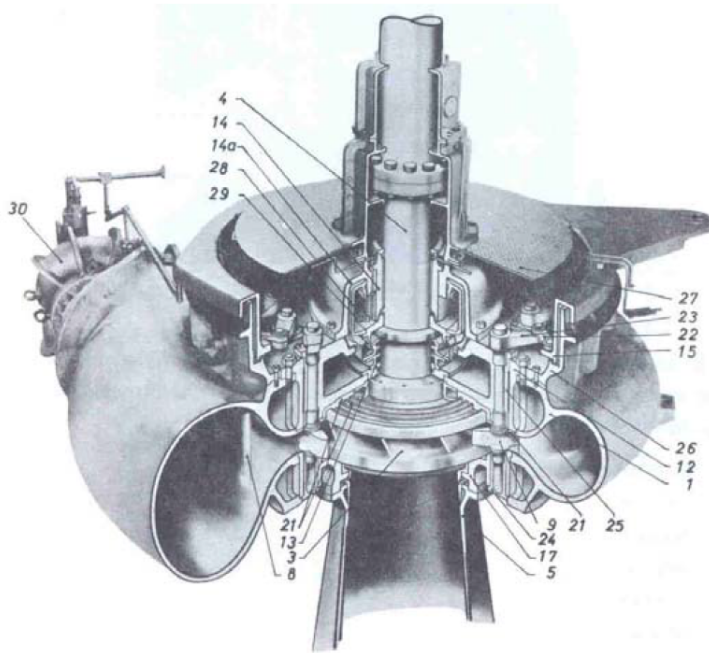
1. The scroll casing	15. Regulating ring	26. Bearing for the regulating
3. Runner	17. Lower cover	ring
4. Shaft	21.Replaceable wear and	27. Floor
5. Draft tube cone	labyrinth rings	28. Rotating oil cylinder
8. Stay vanes	22. Link	29. Oil scoop fastened to
9. Guide vanes	23. Lever	(14a) and (14) with the
12. Upper cover	24. Lower bearing for guide	opening against the
13. Sealing box	vane	rotating oil in rotating
14. Guide bearing	25.Upper bearing for guide vane	oil cylinder (28)
14a.Bracket for the bearing(14)		

Figure 1.2.2: Cross section of a Francis turbine [13].

Spiral casing

The spiral casing is the water conduit between the penstock and the regulating mechanism [14]. The cross section through the spiral casing is continuously decreasing, the retardation in cross section causes an equal distribution of water into the guide vane cascade [14, 13].

In older designs the spiral casing was usually casted. For new designs it is commonly made by plate segments welded together. This has decreased the production cost

and the transport expenses considerably [14] without noticeably decreasing the efficiency [15].

For vertical axis Francis turbines the spiral casing is usually embedded in concrete for increased support [14].

Stayring and stay vanes

The stay ring consist of an upper and lower ring connected by welded stay vanes. The stay vanes purpose is to absorb the axial forces on the inside of the spiral casing [14]. The vanes are given a favourable hydraulic shape to affect the water flow minimally.

Regulating mechanism

The regulating mechanism consists of guide vanes, vane arms and links [13]. The purpose of the mechanism is to regulate the flow of water into the turbine. The regulating mechanism is controlled by a governor system that controls a servo motor connected to the guide vanes. A normal connection system is to have the guide vane links connected to a control ring which again is connected to the servo motor. The guide vane rotates around a shaft changing angle so the correct relative velocities can be obtained at different mass flows. The guide vanes are shaped according to hydraulic requirements and should be given a smooth surface [14]. The guide vane shafts are supported by bearings in the upper and lower cover. The bearings are often plain bearing with teflon coating to avoid the need for external lubrication [14]. When the guide vanes are in closed position they overlap by a factor set between 10 and 15 percent [16]. Together with the governor the adjustable guide vane mechanism makes it possible to deliver power with a stable frequency to an electrical distribution grid [14, 13].

Covers

The pressure head limit for a Francis turbine is mainly determined by the clearance between the guide vanes and the covers [11, 17]. Large clearances will lead to large losses and decreased efficiency. The covers should therefore be designed with sufficient rigidity so the deformation remains small when pressurised [17], this also applies to the guide vanes. More rigid covers leads to larger dimensions and higher material costs. The highest profitable head for a Francis turbine will therefore be about 800 m [17].

Runner

The runner consists of a hub, a shroud and runner blades connecting them. The runner converts the energy in the water to rotating motion and torque. The torque is transferred to the turbine shaft through a bolted friction joint or a combined friction/shear joint [14]. The runner can either be casted or welded. For a welded design the hub and shroud is usually cast and welded together with hot pressed plate vanes [14]. The number of blades depends upon the operating head. Runners with higher head will require a higher number of blades, this is mainly because of strength consideration [17]. Increasing the number of blades reduce the pressure

loading on the blade which will help to avoid cavitation and also prevent separation at the runner inlet during low loads [17]. An increase in the number of blades also leads to more contact surface through the runner and thereby an increase in the friction losses [17].

The thickness of the runner blades has to be large enough to withstand the hydraulic forces the blade is exposed to. The hydraulic forces are the static pressure between the pressure and suction side of the blade and the dynamic pulsations, the static pressure is the governing force [9]. For high head Francis turbines it is preferred to shape the blade in such a way that the main part of the hydraulic energy is utilized at the beginning of the blade. In this area the pressure difference from the pressure to the suction side will be large and thereby also the forces on the blade. It is therefore usual to have an increased thickness of the blade near the inlet and let the blade get thinner towards the outlet [3].

Labyrinths

There will always be a gap between the runner and the turbine covers. Water leaking through these gaps will cause reduced efficiency since it will not be utilized by the runner. To decrease the amount of water through the gap obstacles can be placed in the water way. By leading the water through a labyrinth there will be a pressure drop and thereby less leakage. The labyrinth can be constructed to alter the direction of the water, or to increase and decrease the cross section of the flow. Both methods will remove energy from the water and decrease the pressure. The leakage flow through the seals depends upon the size of the gap. In sand laden water the labyrinth seals are exposed to wear. For a new turbine the labyrinth gap will be small and the leakage will be low. As the seals wear the gap increases and so does the leakage [14]. The labyrinth usually consists of two parts, a static seal connected to the covers and a rotating part connected to the runner.

The smallest distance between the runner and the cover is usually placed in the labyrinth and this is where shearing will occur in case of instability. By designing the labyrinth slightly conical with the smallest section downstream the runner will become self stabilizing and the chance of shearing will be reduced [18].

The labyrinth seal also function as a filter. For high head turbines the leakage water may be utilized as cooling water after it has been filtered through the labyrinth seal and thereby increasing the overall efficiency of the turbine [14].

Draft tube

The draft tube is the water conduit from the runner to the outlet gate. Its purpose is to convert the kinetic energy at the runner outlet to pressure energy at the draft tube outlet [13]. This is possible by leading the water through a channel with increasing cross section [19].

The draft tube consists of a cone and a plate shroud. The draft tube cone is of welded plate design and normally consist of two parts, upper and lower cone. For units dismantled from below, this design is always used [14]. The upper part of

the cone is mounted to the lower cover. The lower cone is normally designed as a dismantling piece. This is connected to the draft tube shroud by a flange [14].

The draft tube for Francis turbines is usually designed with a bend. The water through the draft tube is continuously decelerating. Through a bend a decelerating flow may cause problems with separation and cavitation. Due to this the cross section is usually decreased slightly upstream of the bend to accelerate the water and avoid separation [20]. After the bend the cross section is often converted to a rectangular shape towards the outlet [19].

To avoid separation and back flow the angle between the center line and the draft tube wall should not be higher tan 3 degrees [21]. If the angle is to large separation may occur and the draft tube looses its effect [20].

The effect of removing the draft tube depends on the head of the turbine. For a high head Francis turbine the change in efficiency may be less than 1% while removing the draft tube of a low head Kaplan turbine may reduce the efficiency with more than 50% [19].

Hydraulic forces on Francis runner

Figure 1.2.2 shows the hydraulic forces acting on the Francis runner [20].
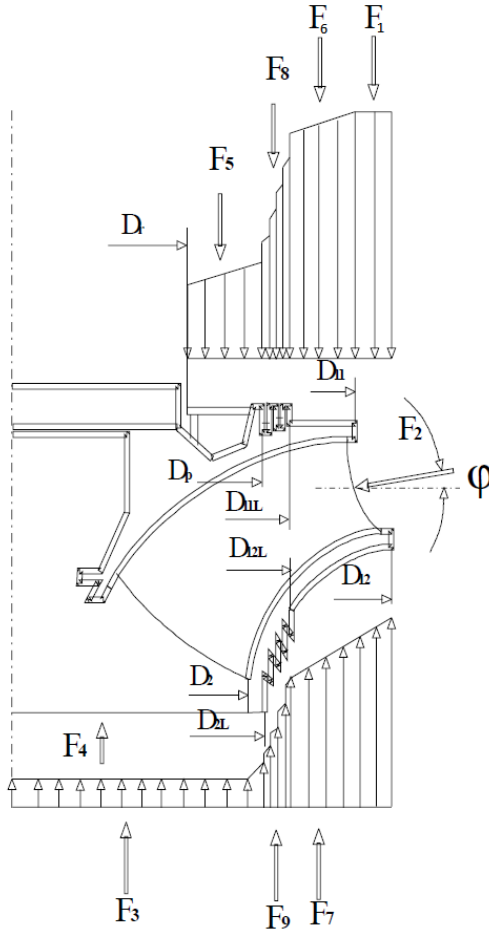
Figure 1.2.3: Hydraulic forces acting on a Francis runner [20].

- F_1 is the force acting on the shroud caused by the difference in diameter on the hub and shroud.

- F_2 is the reaction force at inlet due to the flows axial velocity component.

- F_3 is caused by the pressure in the outlet.

- F_4 is the reaction force at the outlet.

- F_5 is is caused by the pressure between cover and the runner on the inside of the labyrinth seal.

- F_6 and F_7 is caused by the pressure between the covers and the runner outside the upper and lower labyrinth seal.

- F_8 and F_9 is the forces on the upper and lower labyrinth seal.

Simplified calculations of all the forces can be found in Brekke [20].

Pressure distribution between the covers and the runner

The absolute velocity between covers and the runner is assumed to be about 50% of the periphery velocity of the runner [20]. By velocity measurements the absolute velocity, c_u, have been measured to be between 0.5-0.55 times the periphery velocity [20]. Equation 1.2.1 shows how the tangential absolute velocity over the runner can be calculated.

$$c_u = k \cdot r \cdot \omega \; [m/s] \tag{1.2.1}$$

k is an empirical value set between 0.5 and 0.55 [20]. By inserting Equation 1.2.1 in to an equation of balancing of forces for a fluid element equation 1.2.2 is obtained [20].

$$\frac{\partial h}{\partial r} dr = \frac{c_u^2}{g \cdot r} dr \rightarrow \frac{\partial h}{\partial r} = \frac{k^2 \cdot \omega^2 \cdot r}{g} \; [-] \tag{1.2.2}$$

By integrating equation 1.2.2 from the labyrinth ring to the inlet, Equation 1.2.3 is obtained [20].

$$\int_h^{h_i} dh = \frac{k^2 \cdot \omega^2}{g} \int_r^{r_i} r \cdot dr \rightarrow h_i - h = \frac{k^2 \cdot \omega^2}{2 \cdot g}(r_i^2 - r^2) \; [m] \tag{1.2.3}$$

The pressure at the seal depends on the drainage system. If the leakage water is used for cooling, the water can be drained right after the labyrinth and the pressure will be the same as the cooling water pressure [20].

If the system uses a pump plate the pressure will decrease between the labyrinth and the lowest diameter of the pump plate [20]. The pressure distribution between the upper labyrinth and the shaft seal can be found the same way by integrating from the seal to the labyrinth. This gives Equation 1.2.4 [20].

$$h(r) = h_p - \frac{k^2 \cdot \omega^2}{2 \cdot g}(r_p^2 - r^2) \; [m] \tag{1.2.4}$$

1.2.3 Material choice for Francis turbines

Francis turbine components are categorized in two parts, pressurized static parts and movable stressed parts. The pressurized static parts include the spiral casing, top and bottom cover, stay ring, and draft tube. The movable stressed parts includes guide vanes, shaft, runner and labyrinth seals. For high head turbines the stress carrying parts like the guide vanes and runner blades are made from micro alloy steel, also known as *fine grain high tensile strength carbon steel*, to decrease the thickness without increasing the danger of fracture. The maximum stress and numbers of pressurizing cycles are the basic for design and choice of materials for these parts. The covers and draft tube are made from *fine grain low tensile stress with low carbon content steel* for defect free welding [4]. Table 1.2.1 shows the operating conditions and material choice for the different parts. The material choice in Table 1.2.1 is based upon experience from Norwegian power plants [4].

In the guide vanes it is normal to use $13Cr1Ni$, for high head turbines it can be replaced by the stronger $13Cr4Ni$. A material with higher hardness should be chosen for the head and bottom cover to avoid severe shearing between the covers and guide vanes, a difference of 70HB is recommended as a minimum [10].

Table 1.2.1: Materials used in Francis turbines [4].

Part	Operating condition and requirements	Material
Guide vane	High velocity, prone to cavitation, corrosion, sand erosion	13Cr4Ni
Runner	High velocity, prone to cavitation, corrosion, sand erosion	16Cr5Ni
Upper part of draft tube	High velocity, prone to cavitation and corrosion, welding at site	16Cr5Ni
Facing plates	Abrasion or adhesion between guide vanes and facing plates	16Cr5Ni
Labyrinth (static)	Minimum gap to avoid leakage loss, replaceable	Ni-Al bronze (steel in case of erosion)
Labyrinth (rotating)	Minimum gap to avoid leakage loss	16Cr5Ni

1.2.4 Erosion in Francis turbines

The components mainly exposed to erosion are the one exposed to high velocities in combination with high acceleration and turbulence.

In the stay vanes erosion may occur due to secondary flows from the spiral casing causing incorrect flow angles at the inlet [10]. The erosion damage is worst at the connection between the stay vanes and the stay ring [8].

The gaps between the head- and bottom cover and the guide vanes have a large effect on the efficiency of the turbine [10]. Due to cross flow over the guide vane pressure and suction side the connecting surfaces are exposed to sediment erosion [15]. As the gap erodes the efficiency of the turbine decreases due to unfavourable flow conditions at the runner inlet. If there is a gap between the covers and the guide vane in closed position, water will flow through the gap at very high velocity and may accelerate the damage severely [22]. The guide vane bearings are also exposed for erosion. Polluted water can enter through the gap between the covers and the guide vane shaft and cause damage to the guide vane, covers and bearings [15].

The labyrinth seals are also exposed to erosion, eroded seals will increase the gap loss and thereby decrease the efficiency of the turbine as less water will be utilized.

The highest acceleration in the turbine takes place at the runner blade inlet, and the highest relative velocities takes place at the runner blade outlet [23]. Because of the leakage through the gap between the runner and covers, secondary flow may occur and create vortices. When these vortices hit the runner inlet, erosion at the top and bottom of the leading edge of may occur [10].

Design measures to avoid erosion

In a hydraulic power plant there will always be a compromise between several requirements. Design measures that increase the particle abrasion resistance may affect other aspects of the turbine negatively.

Table 1.2.2: Measures to increase abrasion resistance with advantages and disadvantages [22].

Measure	Advantages	Disadvantages
Thicker runner blades	Increased time before the erosion causes the structural integrity of the runner to be compromised.	Decreased efficiency and increased risk of vibrations caused by Von Karman vortices.
Fewer runner blades	Improve access to the flow channel for coating purposes.	May result in reduced cavitation performance.
Increasing runner diameter	Decrease relative velocity of the water through the runner	Increase space requirements and material costs.
Coating on exposed parts	Increased abrasion resistance of the surface.	May increase the surface roughness, which may reduce the efficiency.

Table 1.2.2 lists some of the measures possible to reduce erosion. It is however important to remember that every measure taken increases the total cost of the power plant and have to be weighed against the total gain.

1.3   Numerical analysis

1.3.1   Computational Fluid Dynamics

CFD is a computer based tool used to simulate fluid flow, heat transfer and other physical processes connected to fluid behaviour [24].

History

Computers have been used to solve problems with fluid dynamics for several years. In the 70s, the complex mathematics required to generalize the algorithms began to be understood and general purpose CFD solvers were developed [24]. These solvers did however require, what was then, very powerful computers and were soly used for research. In later years the advances in computer power combined with powerful graphics and 3D-models have made the process of creating CFD models and analysing the results much more intuitive and less time consuming. CFD also offers an alternative to expensive laboratory testing. As a result of this, CFD has now been well established as an industrial design tool [11, 24].

Mathematics

In a CFD analysis the differential equations describing the processes of momentum, heat and mass transfer, known as the Navier-stokes equations are solved. Also other equations describing processes like combustion and turbulence are included in the solvers [24]. There are several different solution methods that are used in CFD codes. The most common is known as the *finite volume technique*. In this technique the region of interest is divided in to small control volumes. The equations is then discretized and solved iteratively for each control volume. Different solvers uses different forms of the equations. ANSYS CFX solves the unsteady Navier-stokes equations in their conservative form [24].

1.3.2   Finite Element Method

The Finite element method (FEM) is a powerful tool used to solve the boundary conditions of continuum [11]. The method is widely used in the analysis of hydraulic turbines [11]. The method is used in stress and strain analysis, eigenvalue analysis, dynamic response analysis and flow analysis [11]. The FEM discretization process transforms partial differential equations into algebraic equations [25]. In FEM the structure of interest is divided in to several small elements. The variables of the governing differential equations and their derivatives are specified at the nodes at the edges of each element. The solution is dependent on the quality of the grid. There is no general rule for division of elements or grid generation, but size and arrangement of the grid is important in practice [11]. It is desirable with fine grids in areas of stress concentration. Elements with very slender proportions should be avoided [11].

When the final element method is applied to three dimensional problems, the number of elements will often become very large and the calculations will require considerable computer time [11].

Computer aided FEM calculations should always be verified by simplified estimations [10].

1.3.3 Fluid Structural Interaction

FSI is the coupling of solution fields in fluid and solid domains [24]. When solving an FSI problem there is two options. An unidirectional (one way) analysis is performed by running a CFD analysis, extracting the forces acting on a solid surface and then importing them to a structural analysis. In an unidirectional analysis the response from the structural analysis will not affect the CFD analysis [24]. In a bidirectional (two-way) analysis the structural response will be taken into account and affect the flow simulation.

1.3.4 Errors and uncertainties in numerical modelling

In the context of thrust and confidence in a numerical model the following definitions of errors and uncertainties have been defined [26]:

Error is defined as *a recognisable deficiency in a numerical model that is not caused by lack of knowledge* [26]. Causes of errors defined this way is [26]:

- Numerical errors: Round of errors, iterative convergence errors, discretisation errors.

- Coding errors: Mistakes or "bugs" in the software.

- User errors: Human errors through incorrect use of the software.

Uncertainty is defined as *a potential deficiency in a numerical model that is caused by lack of knowledge* [26]. Causes of uncertainties defined this way is [26]:

- Input uncertainty: Inaccuracies due to limited information or approximate representation of geometry, boundary conditions, material properties etc.

- Physical model uncertainty: Discrepancies between real flow and the numerical model due to inadequate representation of physical or chemical processes(e.g. turbulence, combustion) or due to simplifying assumptions in the modelling process (Steady state, incompressible flow etc.).

The solution of numerical models depends upon the solver grid. If computational resources allows it, it is always recommended to adapt the grid until the solution is independent of the mesh [24]. When grid independence is obtained, a coarse, independent mesh should be used to save computational resources in further analyses [24]. For CFD models a fine grid resolution walls is required close to walls to obtain

a good solution for the boundary layer [24]. A non-dimensional wall distance can be defined like in Equation 1.3.1 [24].

$$y^+ \equiv \frac{u_\tau \cdot y}{\nu} \ [-] \qquad (1.3.1)$$

u_τ is the friction velocity at the nearest wall, it is defined as $u_\tau \equiv \sqrt{\frac{\tau_w}{\rho}}$. y is the distance from the node to the nearest wall. ν is the local kinematic viscosity. Different turbulence models have different $y+$ requirements [24]. For the Shear Stress Transport (SST) model the requirement is $y+ < 2$ while for the *k-epsilon* model $30 < y+ < 300$ [24].

Chapter 2

Method

2.1 FSI analysis of Francis runner

The geometries used in the analyses were drawn in the CAD program *Pro/Engineer*. The FSI analyses were performed by combining CFD analyses in *ANSYS CFX* and FEM analyses in *ANSYS Static structural*. The connection between the different programs were done in *ANSYS Workbench*. Figure 2.1.1 shows the workbench connections.

The FSI analyses performed were unidirectional, meaning that the deformations in the structure caused by the forces from the fluid were not taken in to account in the flow analysis.
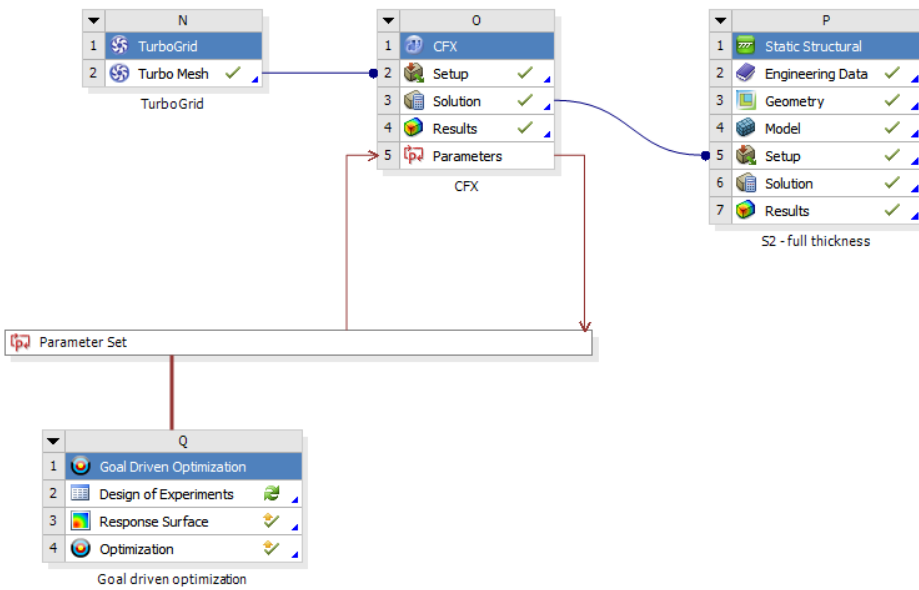

Figure 2.1.1: FSI Analysis layout in ANSYS workbench.

2.1.1 CAD of Francis runner section

The reference runner consists of 17 identical sections. For each of the designs one section was modelled. The modelling was done by importing curve files for the blade, hub and shroud from Khoj. Quilts were drawn between the curves. When they formed a closed section it was made solid by filling in the empty volume between the quilts. Figure 2.1.2 shows the section model for the reference runner, Figure 2.1.3 shows the runner consisting of 17 sections. A detailed step by step description of the modelling can be found in Appendix I.
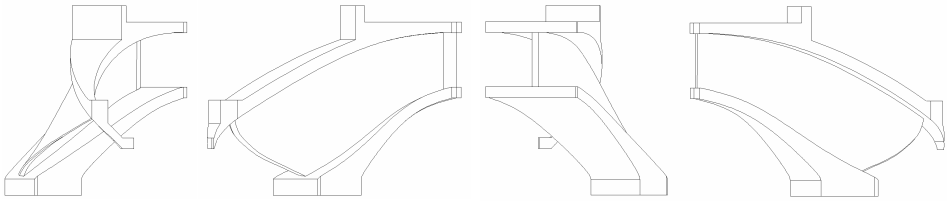

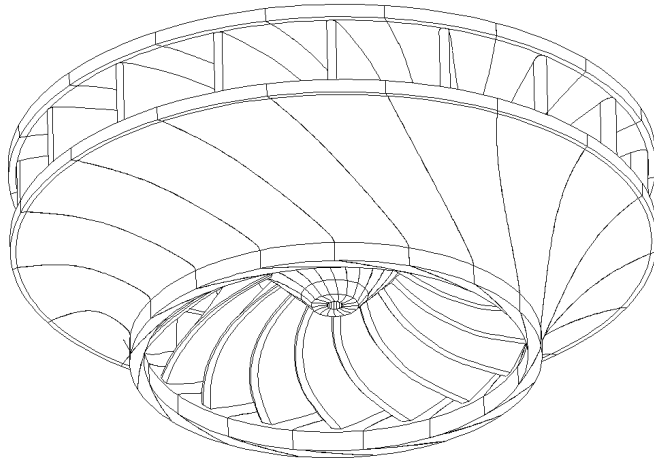Figure 2.1.2: Section of the reference runner modelled in Pro/Engineer.

Figure 2.1.3: Reference runner consisting of 17 sections modelled in Pro/Engineer.

2.1.2 CFD Analysis

Meshing

The meshing was performed in *ANSYS TurboGrid*. *ANSYS TurboGrid* is a meshing tool that is specialized for CFD analyses of turbo machinery blade rows [24].

Curve files defining the hub, shroud and blade were imported into *TurboGrid*. The curves were created in *Khoj*. The number of blade sets were set to 17.

The Topology definition setting govern the general way the mesh is generated [24]. The placement and method setting were set to *ATM Optimized*. ATM optimized topology is the default in *TurboGrid*. According to ANSYS, ATM enables you to create high quality meshes with minimal effort as there is no need for control point adjustment [24].

For the boundary layer refinement control the *First element method* was used. An offset y+ of 1 was used with the *Near wall element size specification*, this was done so the mesh would meet the y+ requirement for the turbulence model. The domain was set to *Outlet domain*.

The mesh size was defined by the *Target passage mesh size* method. The node count was increased until satisfactory y+ values were obtained in *CFX Post*.

Flow analysis in ANSYS CFX

The CFD analysis were performed in *ANSYS CFX*. The mesh from *ANSYS TurboGrid* was imported through ANSYS Workbench. The set-up was performed in *CFX TurboMode*. Machine type were set to *Radial turbine*. Component type was set to *Rotating* with -1000 rpm. In *Passages and alignment*, *Passages to model* was set to 3. *Theta offset* was set to $-\frac{360}{17}$, this was done so the middle blade in the CFD analysis would share the coordinates with the CAD model.

As boundary conditions at inlet and outlet, mass flow at inlet and static pressure at outlet were chosen. The other surfaces are given boundaries as *Domain interface* or walls automatically by *TurboMode*. At the inlet the flow direction were given in cylindrical coordinates. The radial and tangential velocity components were defined by equations named V_r and V_t.

k-epsilon was chosen as the turbulence model. *k-epsilon* is consdiered the industry standard due to its numerically robustness and predictive capability [24]. The *k-epsilon* model offers a good compromise between accuracy and robustness [24].

To obtain the correct head an iterative method was used by changing the inlet angle. In *CFX post* the inlet head was set as an output parameter. In *CFX Pre* the radial velocity, V_r, was set as an variable an defined as a CFX input parameter. The angular velocity, V_t, was defined by equation 2.1.1.

$$V_t = \sqrt{1 - V_r^2} \qquad\qquad (2.1.1)$$

The initial values used were obtained from the turbine data file from *Khoj*.

By using *Goal driven optimization*, simulations of five different design points around the initial value were performed. From the results *Goal driven optimization* suggested three different input values for V_r to obtain the correct head. The values that were closest to correct head were used for further analyses. Table 2.1.1 shows the different cases analyzed.

Table 2.1.1: CFD analysis parameters.

Design	Thickness leading/ trailing edge(mm)	Operational conditions	Volume flow (m^3/s)
Reference	15/8	Best point	2,35
S1	15/8	Best point	2,35
S2	15/8	Best point	2,35
Reference	10/6	Best point	2,35
Reference	10/6	Full load	2,82

Verification and validation of results

To verify the solution from the CFD analysis a mesh independence analysis was performed. Three nodes measuring velocity were placed along the trailing edge of the center blade to check for transient behavior in the steady state analysis. A short transient analysis was performed on blade design S1 to prove transient behavior.

To validate the results the shaft power, mass flow, efficiency and head were set as output parameters and monitored for the different results. The shaft power was also calculated manually and the mass flow were monitored in the solver.

2.1.3   Structural analysis

The meshing and structural analysis of the runner were performed in *ANSYS Static Structural*. A static structural analysis determines the displacement, stresses, strain and forces in structures or components [24].

Meshing

The size of the mesh was controled by using *Body sizing*. Match control was used on the cut surfaces of the geometry. The *match control* matches the mesh on two faces or two edges in a model [24]. The two edges matched must be topologically and geometrically the same. Match control has two options, arbitrary or cyclic matching. In this case cyclic matching was used.

Boundary conditions

Figure 2.1.4 shows the boundary conditions set in Ansys mechanical. The cyclic symmetry boundary condition is not shown on the figure.
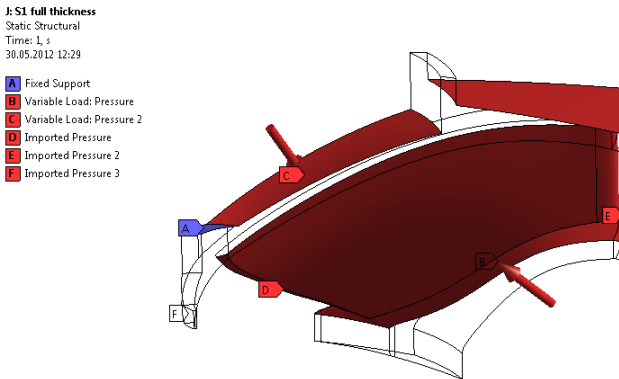

Figure 2.1.4: Boundary conditions for the reference runner.

The boundary condition *Fixed support* was used on the connecting surface between the hub and shaft, also the surface were the bolts will be placed were defined as a *Fixed support*.

The pressure distribution between the inlet and the upper labyrinth on the top side of the hub and underside of the shroud were given by Equation 2.1.2. A cylindrical coordinate system where $x = r$ was placed in origo of the global coordinate system.

$$p(r) = p(x) = \rho \cdot g \cdot h(x) = (\rho \cdot g)(h_i - \frac{k^2 \cdot \omega^2}{2 \cdot g}(r_i^2 - x^2)) \ [Pa] \qquad (2.1.2)$$

At the surface of the hub between the shaft and upper labyrinth seal, the pressure was given by Equation 2.1.3.

$$p(r) = p(x) = \rho \cdot g \cdot h(x) = (\rho \cdot g)(h_p - \frac{k^2 \cdot \omega^2}{2 \cdot g}(r_p^2 - x^2)) \ [Pa] \qquad (2.1.3)$$

The values for the parameters in Equation 2.1.2 and 2.1.3 is found in Table 2.1.2.

Table 2.1.2: Boundary condition parameters.

Parameter	Value
ρ	$997 kg/m^3$
g	$9,81 m/s^2$
h_i	$92,7m$
h_p	$0,011m$
r_i	$0,455m$
r_p	$0,0876m$
k	$0,5$
ω	$104,7s^{-1}$

The derivation of Equation 2.1.2 and 2.1.3 can be found in Chapter 1.2.2.

Inside the channel the pressure field from the CFD analysis were imported by to the surfaces of the blade, hub and shroud. The boundary condition for the cut faces on the hub and shroud were given by using cyclic symmetry. This was done by inserting *Commands (APDL)* and including the following command lines:

$\backslash prep7$
$cyclic, a$
$cycopt, facetol, b$
$\backslash solu$

Cyclic defines the cyclic analysis where a is the number of identical cyclic elements, in this case $a = 17$. b is the tolerance angle for face matching in the cyclic analysis, if nothing is defined b is set to 15 degrees by default, in this case $1 < b < 5$ depending on the mesh. For the meshes with 5 mm body sizing and match control, matching was obtaied with $b = 2$. According to ANSYS [24] the required tolerance angle for advanced geometries may be between 5 and 10 degrees.

Verification and validation of results

To verify the solution from the *Static structural* analysis a mesh independence analysis was performed with five different meshes. The details for the different meshes can be seen in 2.1.3. The statistics for the final mesh was checked against the recommended values from *ANSYS meshing guide* [27].

Table 2.1.3: Mesh independence analysis for structural analysis

Mesh	Element size (mm)	Number of nodes	Functions
1	5	301254	Match control, Body sizing
2	4	570058	Match control, Body sizing
3	-	520089	Match control, Advanced sizing: proximity and curvature(Coarse)
4	-	674442	Match control, Advanced sizing: proximity and curvature(Medium)
5	-	737826	Match control, Advanced sizing: proximity and curvature(Fine)

The results were validated by comparing the deformation and stress distribution to a simplified method described in Brekke [10]. A simplified stress calculation were performed using Equation 2.1.4 and 2.1.5 [10].
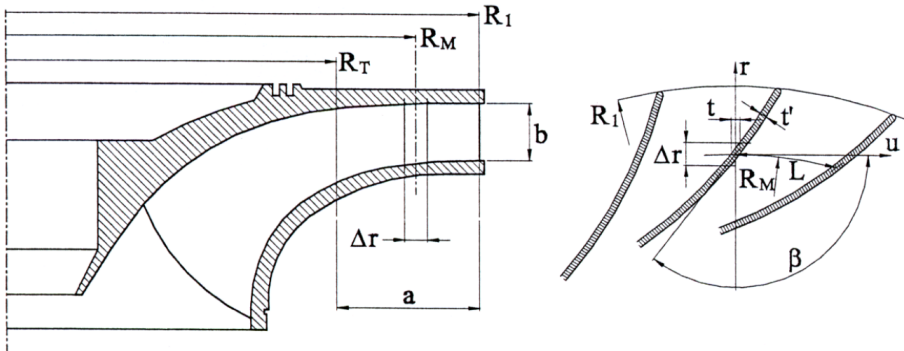

Figure 2.1.5: Principal sketch of Francis runner [10].

Figure 2.1.5 shows a sketch for a high pressure Francis turbine. In this method it was assumed that all of the torque was transferred from the water to the turbine between R_t and the outer radius, R_1. The moment arm is then $R_m = \frac{R_t + R_1}{2}$.

Table 2.1.4: Parameters for simplifed stress calculation

Parameter	Symbol	Unit	Value
Power	P	W	4,2e6
Number of blades	Z	-	17
Outer radius	R_1	m	0,445
Inlet height	b	m	0,097
Blade thickness	t	m	0,015 & 0,010
Angular velocity	ω	s^{-1}	104,7

$$\Delta p = \frac{P}{ZabR_m\omega} \tag{2.1.4}$$

$$\sigma = \frac{6M}{\Delta rt^2} = \frac{2b^2\Delta p}{t^2} \tag{2.1.5}$$

In this case it was assumed that all of the torque was transferred from the leading edge to the middle of the blade, i.e. $R_t = \frac{R_1}{2}$.

2.2   CAD of Francis turbine

The model from the authors project thesis [5] was redrawn. All main dimensions was parametrized by referring the names of lines and arches in *Sketch mode* to *Relations*. All adjacent faces were connected by using *Publish Geometry* and *Copy Geometry*. By using this method, parts will automatically follow changes in adjacent parts.

The spiral casing was modelled by importing the center line from *Khoj*. A variable section sweep along the center line and a constant inner radius with a circular section was performed. This gave a quilt formed as a closed spiral casing without thickness. The quilt was given thickness by using the function *thicken*. The stay ring geometry was imported and revolved with the function *remove material* to make an opening for the stay ring. An extension towards the penstock with a flange was added.

The draft tube cone was modelled by importing the geometry for the lower cover and revolving a 2D sketch. The draft tube bend was modelled by importing the cone geometry. Two axes were added, one at the back of the cone outlet and one in the center. A datum plane with an angular offset from the top plane was placed through the center axis. A sketch representing the center curve of one section of the bend was drawn in the new plane. A new axis was placed at the end of this line. A datum plane was placed through the axes at the back of the cone and end of the line. A new curve was drawn in this plane representing the radius of the cross section of the bend. *Variable section sweep* with a half circle with center on the center curve and end point in the radius curve was used to create one circular section of the bend, Figure 2.2.1 shows this step. This section was mirrored through the front plane. *Boundary blend* was used to close the gap between the sections, see Figure 2.2.2. *Thicken* was used to give the tube shell thickness.

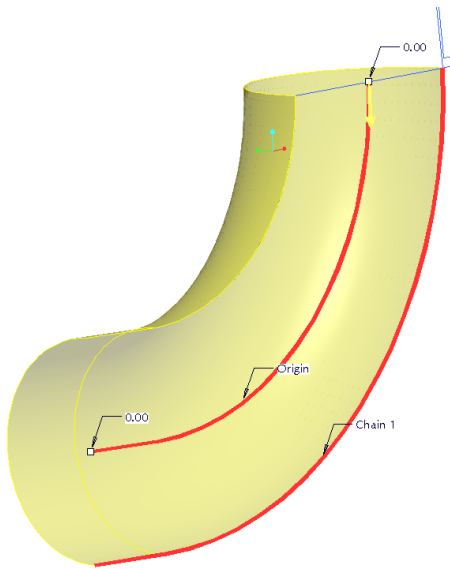For more details about the modelling, see the authors project thesis [5].

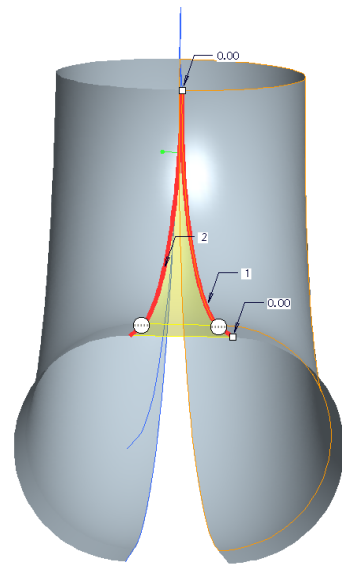Figure 2.2.1: Variable section sweep of draft tube.

Figure 2.2.2: Boundary blend between the draft tube sections.

Chapter 3

Results

3.1   FSI Results

3.1.1   CAD results

Figure 3.1.1 and 3.1.2 shows the top view and front view of the Reference, S1, and
S2 designs with 15 mm thickness at the leading edge and 8 mm at the trailing edge.
The reference design was also drawn with a thickness of 10 mm at the leading edge
and 6 mm at the trailing edge. All the blades were modelled with a unique section
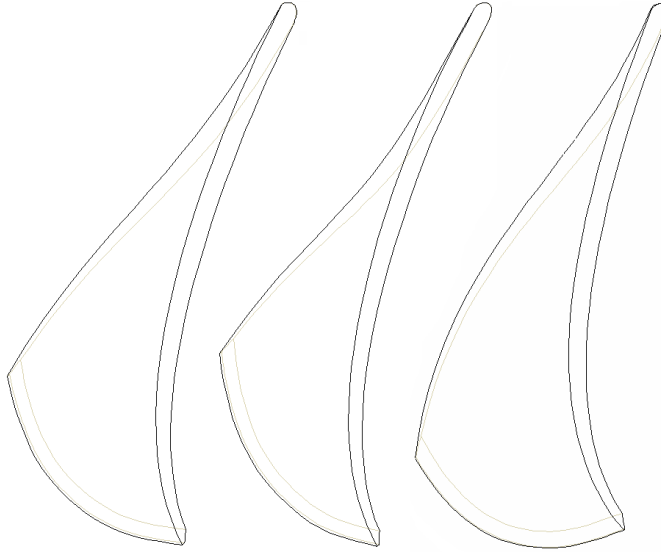of the hub and shroud as seen in Figure 2.1.2.

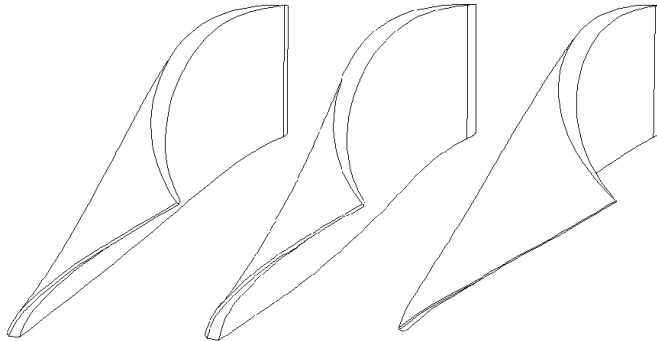Figure 3.1.1: Top view of the Reference, S1 and S2 design.

Figure 3.1.2: Front view of the Reference, S1 and S2 design.

3.1.2   CFD results

Figure 3.1.3 shows the pressure distribution through the blade channel for the reference design.
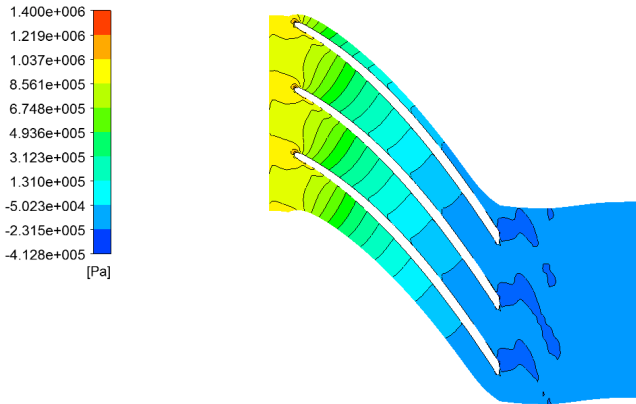

Figure 3.1.3: Pressure distribution through blade channels in the reference design.

Goal driven optimization results

Table 3.1.1 shows the velocities obtained by *Goal driven optimization* used in the final simulations.

Table 3.1.1: Results from goal driven optimization.

Design	V_r	Head(m)	Power(MW)
Reference normal thickness	0,2460	199,6	4.135
Reference reduced thickness	0,2483	201,5	4.157
Reference reduced thickness full load	0,3095	201,5	5.093
Design S1	0,2485	201,52	4.192
Design S2	0,2563	201,5	4.294

Table 3.1.2 shows the results for five design points for the optimization of the reference design. These results were used to obtain the values in Table 3.1.1.

Table 3.1.2: Results from the five design points in the goal driven optimization process.

Design point	V_r	Head (m)	Mass flow (kg/s)	Shaft power (MW)	Efficiency (%)
1	0,245	202,55	7028,9	12,45	97,2
2	0,2205	224,48	7028,9	13,92	97,1
3	0,2695	184,941	7028,9	11,10	96,4
4	0,23275	212,585	7028,9	13,14	97,2
5	0,2572	192,709	7028,9	11,79	97,0

Figure 3.1.4 and 3.1.5 shows the streamlines for the reference design before and after optimization.
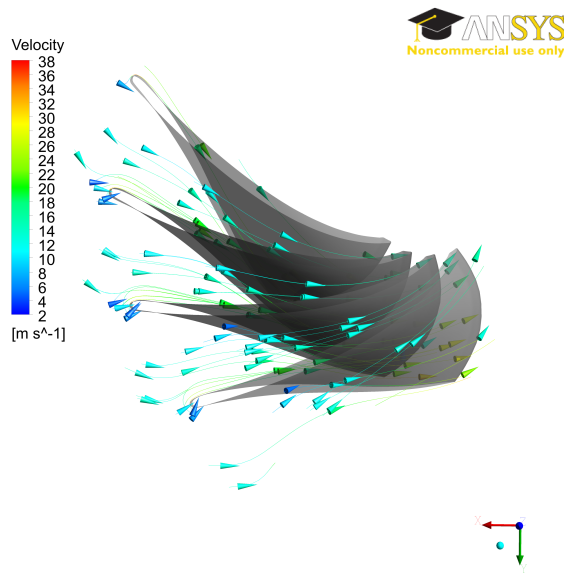
Figure 3.1.4: Streamlines for the reference design with velocity components from Khoj.
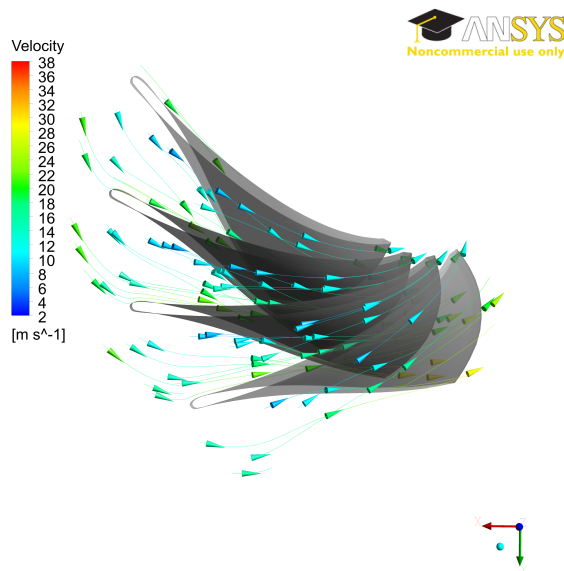

Figure 3.1.5: Streamlines for the reference design with velocity components obtained with Goal driven optimization.

Verification and validation of results

Mesh independence

Table 3.1.3 shows the results for the mesh independence analysis of the *Turbogrid* mesh. The torque in the table is the torque around the z-axis for three blades.

Table 3.1.3: CFD mesh independence results.

Mesh	Total nodes	Torque(kJ)	
		k-epsilon	SST
1	111596	7.010	-
2	226200	6.977	6.920
3	330693	6,690	-
4	539640	6,967	-
5	1068000	6.972	6.946

Velocity monitoring at trailing edge

For some of the design points the residue did not reach the target of 1e-4, but started oscillating around 5e-4. For the same cases the velocity monitors at the trailing edge were oscillating. Figure 3.1.6 shows the monitoring of the residue and the velocity monitor points placed at the trailing edge.

Figure 3.1.7 shows the residue for the transient analysis using the solution file from the analysis shown in Figure 3.1.6 as initial conditions. The residue reached the target after a few time steps.
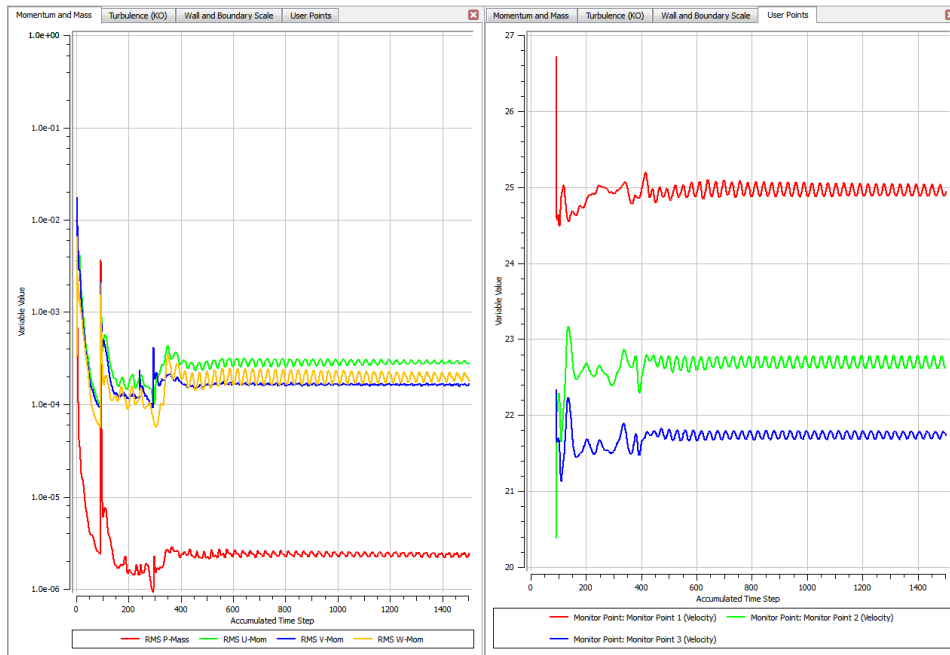
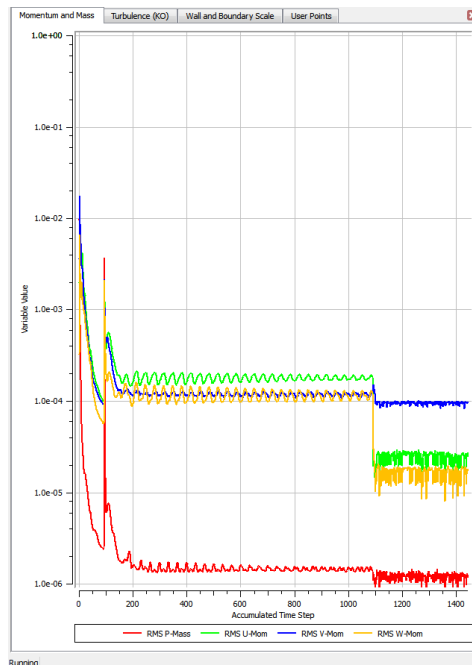Figure 3.1.6: Monitoring of residue and velocity in S1 design point 4.

Figure 3.1.7: Transient analysis of S1 design point 4.

3.1.3 Structural analysis results

Stress distribution in reference design, S1 and S2

Figure 3.1.8 shows the stress distribution in the reference runner. Figure 3.1.9, 3.1.10 and 3.1.11 shows the stress distribution in the Reference, S1 and S2 blade designs with 15 mm thickness at the leading edge and 8 mm thickness at the trailing edge at best point. Figure 3.1.12 and 3.1.13 shows the stress distribution in the reference design with 10mm/6 mm thickness at best point and full load.
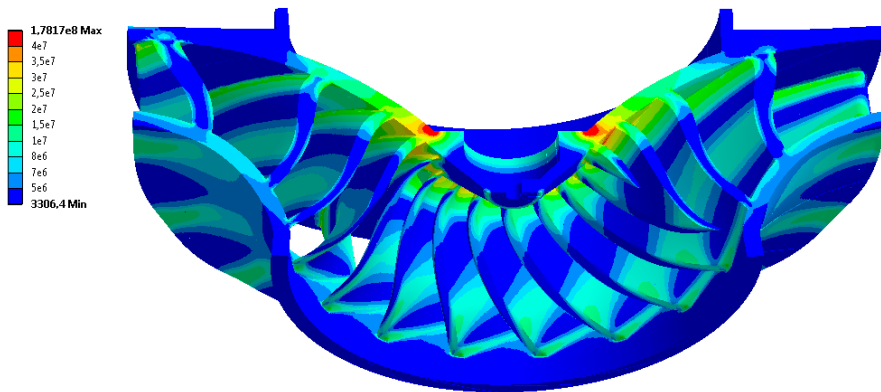

Figure 3.1.8: Stress distribution in the reference runner design. Legend shows Von-Mises stress in Pascal.
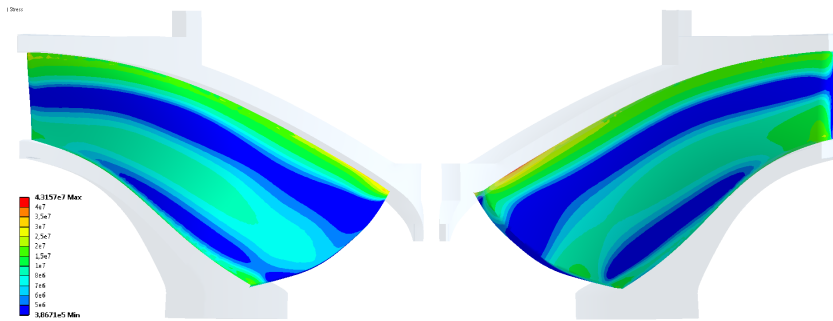
Figure 3.1.9: Stress distribution in the reference blade design. Legend shows Von-Mises stress in Pascal.
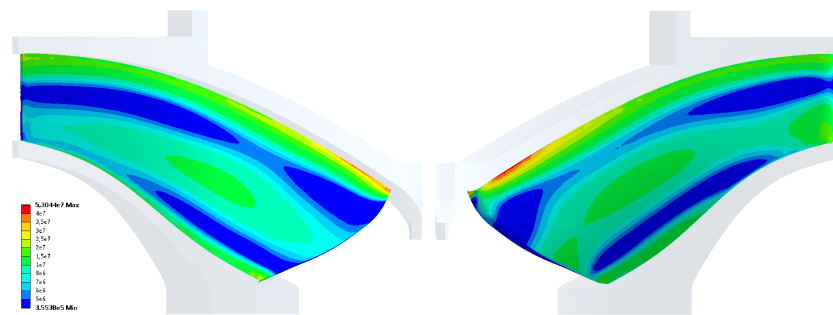

Figure 3.1.10: Stress distribution in the S1 blade design. Legend shows Von-Mises stress in Pascal.
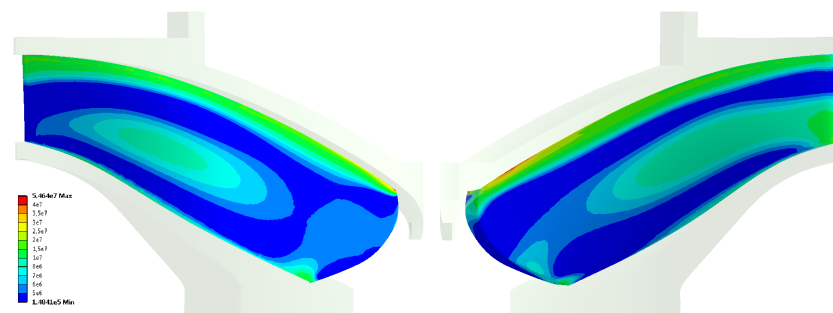
Figure 3.1.11: Stress distribution in the S2 blade design. Legend shows Von-Mises stress in Pascal.

Figure 3.1.12: Stress distribution in the reference blade design with 10 mm thickness at the leading edge and 6 mm thickness at the trailing edge. Legend shows Von-Mises stress in Pascal.
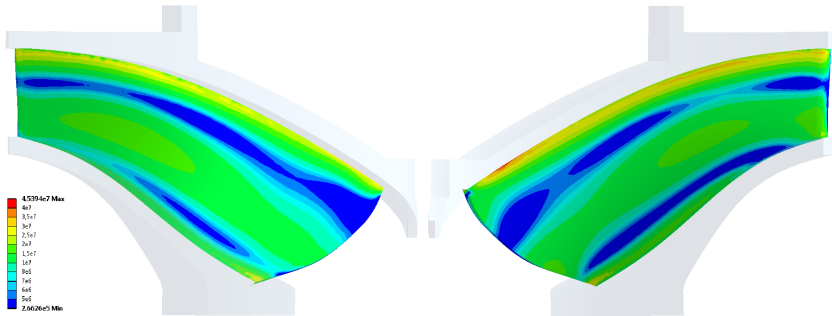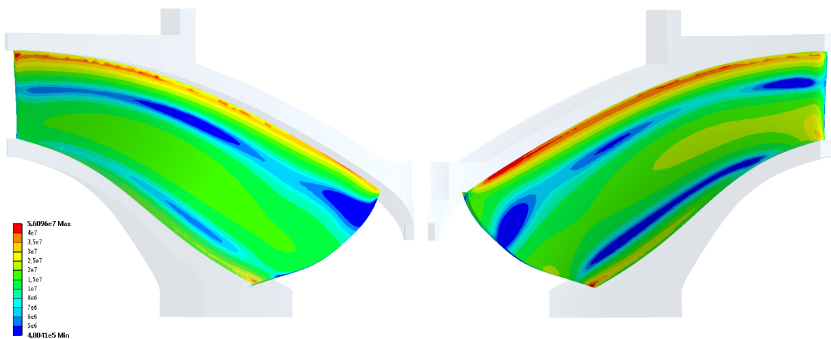

Figure 3.1.13: Stress distribution in the reference blade design with 10 mm thickness at the leading edge and 6 mm thickness at the trailing edge at full load. Legend shows Von-Mises stress in Pascal.

Verification and validation of results

Comparison between structural results and a simplified estimation

The simplified stress approximation with Equation 2.1.5 suggested a maximum stress of 27 MPa for the 15 mm thick blade and 33 MPa for the 10 mm thick blade.

Figure 3.1.14 and 3.1.15 shows the deformation and stress in the reference design compared the simplified method found in Brekke [10].
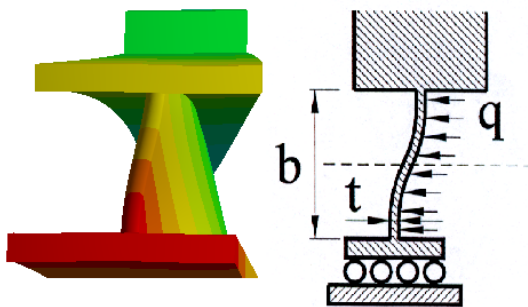

Figure 3.1.14: Comparison between deformation in static structural analysis and expected deformation in a simplified method.
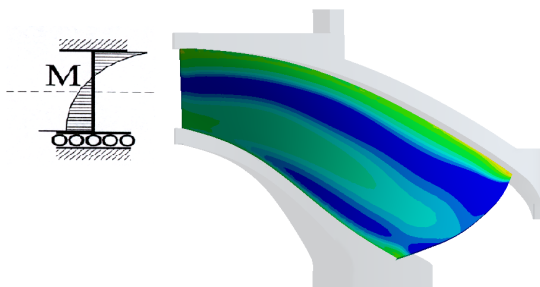

Figure 3.1.15: Comparison between expected moment distribution from a simplified method and stress distribution in static structural analysis.

Mesh analysis

Table 3.1.4 shows the statistics for the final mesh. For more information about the statistics criteria, see ANSYS [27].

Table 3.1.4: Mesh statistics.

Parameter	Target(Best)	Value		
		Min	Max	Avg
Element quality	1	0,08	1	0,825
Aspect ratio	1	1,16	47,8	1,889
Jacobian ratio	-	-100	1,99	1,005

The mesh statistics is from a mesh with an element size of 5 mm and 191761 elements. 191676 of these elements had a Jacobian ratio of 1. Only one element had a Jacobian ratio of -100, it was located at the middle of the trailing edge. Three elements with a high aspect ratio was found in the cut corner of the section. Some elements with low element quality was found on the lower cut surface of the shroud.

Table 3.1.5: Mesh independence results.

Mesh	Max stress (Pa)	Max deformation (m)	Stress node (Pa)	Deformation node (m)
1	1,997e8	0,00014973	6,5616e7	1,2589e-4
2	2,5228e8	0,00015295	6,272e7	1,292e-4
3	1,9169e8	0,00014913	1,5099e8	1,2519e-4
4	1,8046e8	0,000149	1,529e8	1,2507e-4
5	2,1206e8	0,00014866	1,5208e8	1,2472e-4

Several results had to be discarded due to matching problems, Figure 3.1.16 shows
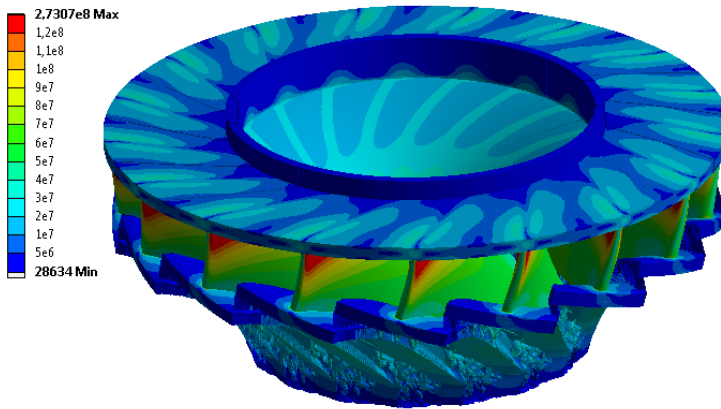an example where all the nodes in the shroud have not been matched.

Figure 3.1.16: Cyclic symmetry analysis of runner with matching problems.

Other results were not as extreme as Figure 3.1.16, but had a few unmatched
surfaces that caused deformations and stress along the cut surfaces.

3.2   New Francis turbine design

Figure 3.2.1 shows the new modified turbine design from the authors project thesis [5]. A spiral casing and draft tube was added to the design. The coated plates were rounded of in the edges to be better suited for coating. the coated plates are fastened by bolts to the covers. A 0.3 mm layer of coating has been applied to the plates in the model. Figure 3.2.2 shows a cross section of the new turbine with the coated plates. The clearance between the runner and covers was increased from 1 mm to 5 mm. The upper stay ring is re-designed to be machined from one piece. The number of guide vanes were decreased from 24 to 20. The runner can be fit to new blade designs by importing new hub and shroud curves.
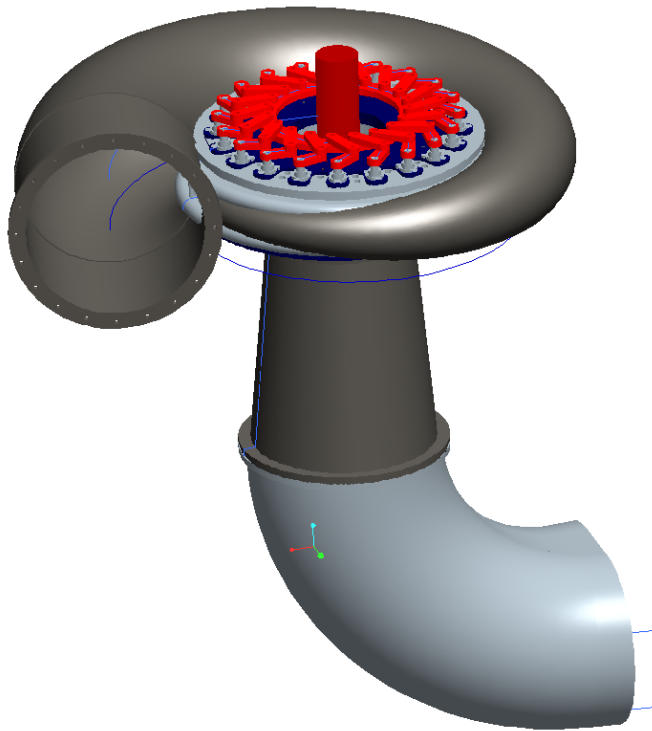
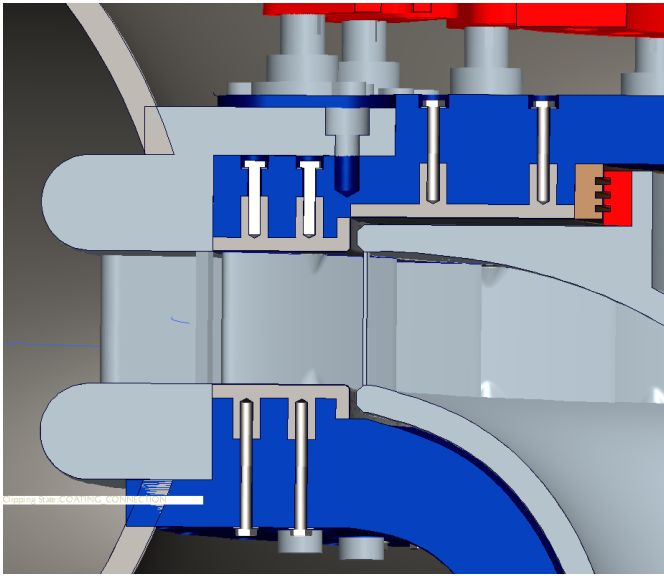Figure 3.2.1: New turbine design for Jhimruk power plant.

Figure 3.2.2: Cross section of the new turbine showing coated plates and connections.

For more details about the design see the authors project thesis *Mechanical design of Francis turbine exposed to sediment erosion* [5].

Chapter 4

Discussion

4.1 FSI Analysis

4.1.1 Method

CAD

To utilize the limited computational power available a $\frac{1}{17}$ section of the complete runner were modelled. The reference design consist of 17 identical blades and the hub and shroud have a constant cross section on the simplified model. On the detailed model there are four holes for the bolts fastening the shaft to the runner. If they were included in the simplified model, the runner would no longer consist of seventeen identical sections. This model would require more computational resources when performing the FSI analysis.

The matching of elements in the structural analysis depended on both the geometry and the mesh. In early attempts the geometry was not accurate enough and matching proved problematic. This was solved by increasing the accuracy in *Pro/Engineer* to maximum and calculating all values outside *Pro/Engineer* to avoid coarse round-off errors. In the early designs a gap of about 0,04 mm were found between the sections when assembling the full runner causing matching problems similar to Figure 3.1.16.

CFD

Due to the ATM optimized topology used in *TurboGrid* meshing, the solution pressure field for an analysis with one blade does not fit the CAD model used in static structural. When imported it will give an asymmetrical pressure field on the hub and shroud. To solve this problem the CFD analysis was performed on three blades with an offset of $\frac{360}{17}$ degrees to align the solution around the middle blade with the CAD model. The pressure field around the middle blade and one half of the blade channel in each direction was imported in the static structural analysis.

The initial velocity components obtained from *Khoj* are calculated for a runner with zero thickness on the runner vanes. This leads to an initial inlet angle that is too small, which again leads to bad flow conditions and an increase in head. By using Goal driven optimization new velocity components were attained giving the correct head and smoother flow conditions.

During the mesh independence analysis the turbulence model k-epsilon was used for all meshes and SST was used for two meshes. When comparing the results from the two turbulence models only small differences were found. k-epsilon was therefore chosen for the rest of the analyses as the $y+$ requirements are lower for this model.

The output from hydraulic turbine report showed a volume flow and shaft power that were 3 times higher than expected. However when the shaft power were

calculated manually in CFX post the results were close to 4,2 MW which was the expected value. The mass flow was monitored during the solution and kept constant at the value given in *CFX Pre*. It is therefore assumed that the values from the hydraulic report were caused by a bug affecting the communication between Turbomode in *CFX Pre* and Hydraulic report *CFX Post* since the meshing in *TurboGrid* was for one blade channel while the simulation was performed on three channels.

For some of the designs the residue started oscillating before reaching the criteria 1.0e-4. According to EDR [28] this may be the result of transient behavior, i.e. turbulence or other unstable flow conditions in the steady state calculations. To validate this assumption nodes measuring the velocity were placed along the trailing edge of the center blade. The results from these measurements showed that there was in fact changes in the velocity. To verify the assumption about transient behavior a transient analysis was performed with the solution file from the steady state analysis. The residue dropped down to the criteria after a few time steps. This proved that the oscillating residue was caused by transient behavior and that there was no complete steady state solution for this exact case.

The mesh independence analysis showed that the maximum difference in torque was 0,6%. The y+ values were within the recommended level for the k-epsilon model for all the meshes. It was therefore not unexpected that the results were similar for all the analyzes.

Structural analysis

Meshing

By using a geometry that represents $\frac{1}{17}$ of the entire runner the number of elements can be increased 17 times and solved with the limited computational power available. It is fair to assume that the solution will have considerably higher accuracy compared to the coarser mesh a full runner mesh would result in.

The mesh analyzed showed some elements with bad statistics. They were few and placed in areas of low interest. It was therefore assumed that the bad elements did not affect the solution considerably.

Mesh independence

The mesh independence analysis showed large differences in local stress. However the general stress distribution and deformation did not differ much between the solutions. A mesh independent solution was not obtained, so local stress should not be considered correct before validating.

The solution of the structural analysis proved to be highly dependent on the mesh. The matching of edges and surfaces in the cyclic analysis depends upon the geometry and the mesh [24]. The analysis showed that it was necessary to apply different face tolerance angles for different meshes. Deformation probes were placed in the

connecting corners of the geometry, and even if the solution appeared to be trust-worthy, the deformation in the connection were often slightly different. On several solutions there were often a few edges that were unmatched and caused bad solu-tions. Some measures is therefore recommended to verify the matching.

- Check if all faces and edges are matched. This is found in the solution output file.

- Inspect the complete runner by using *Visual expansion*. Even if the matching is complete in the output file, it is no guaranty that the solution is correct.

These measures were performed to improve the cyclic symmetry analysis:

- Improved the geometry - increase angular accuracy, create smooth surfaces, decrease the number of adjacent surfaces.

- Improve mesh - use matching along the cut surfaces.

- Adjust angular tolerance for matching.

4.1.2   Results

Stress distribution

The stress distribution in the blade can be explained by simplifying the problem. The hub and shroud is considered completely rigid, the hub fixed and the shroud free to rotate around the center axis but fixed in all other directions. If the blade is considered to be a thin plate the deformation and moment distribution will appear close to the sketches in Figure 3.1.14 and 3.1.15 [20]. When considering the simplified method the highest stress is expected along the hub. High stress is also expected along the shroud. Where the moment is zero the bending stress will be zero. As Figure 3.1.14 and 3.1.15 shows the deformation and stress distribution at the inlet of the blade co-insists with the assumptions from the simplified method. The stress found by using Equation 2.1.5 were close to the stress along the hub seen in Figure 3.1.9 and 3.1.12.

Stress distribution in reference design

The shape of the reference blade is designed to transfer the hydraulic energy to moment evenly across the hole length of the blade. As seen in Figure 3.1.9 the stress was evenly distributed along the blade as would be expected.

Stress distribution in S1

The shape of the S1 blade is designed to transfer the main part of the hydraulic energy from the middle of the blade to the outlet. The blade have a thickness of 15 mm at the inlet and 8 mm at the outlet. I.e. the highest moment will be in the thinner section of the blade. Thereby the stress will be higher than for the reference design where the torque transfer is evenly distributed along the blade.

Comparing the stress distribution to the reference design the trend was the same only shifted towards the outlet.

Stress distribution in S2

The shape of the S2 blade is designed to transfer the main part of the hydraulic energy from the inlet of the blade to the middle of the blade [3]. The blade have a thickness of 15 mm at the inlet and 8 mm at the outlet. I.e. the highest torque transfer will be at the first section of the blade where it is thicker, thereby the stress will be lower compared to designs like the reference design and S1 where the torque is transferred along the blade, also at the thinner outlet section of the blade. S2 also have a higher arch and steeper blade leaning than the Reference and S1 design (see figure 3.1.1 and 3.1.2). This leads to a higher relative thickness when considering the force producing the torque, and thereby lower stress.

Genral

The stress distribution in all the designs with 15 mm thickness at the leading edge and 8 mm thickness at the trailing edge were well within limits. If a safety factor of 5 was considered for structural steel with 600 MPa yield strength, 120 MPa would be the limit. An area with high stress was seen at the hub a bit up from the trailing edge, this was a result of stress from the shaft connection. Figure 3.1.8 shows how the stress from the corner of the shaft effects the blade. In this thesis this area was disregarded as it is caused by a bad hub design, not the blade design.

An analysis of the reference design with 10 mm/6 mm thickness was performed at best point and full load to see if the thickness could be reduced. The stress was, as expected, higher than for the 15/8 mm design, but still well within limits.

For designs like the reference and S1 where the force is distributed more or less evenly along the blade a more even thickness distribution should be considered.

Thinner blades should be considered for all the designs. Thinner blades will leave less friction surface and may increase the efficiency [22]. It may also reduce the risk of vibrations caused by Von Karman vortices [22]. However, for sand laden water erosive wear on the blade should be expected. The erosion will after some time affect the structural integrity of the blade. A compromise between efficiency, material use and erosion resistance should therefore be considered.

4.2   New Francis turbine design

The spiral casing and draft tube modelled in this thesis was of a cast design. Modern designs are usually of welded plate design. A welded plate design reduces the material cost and weight of the turbine considerably and should be considered for this turbine.

Strength calculations were not performed to find the necessary dimensions for the bolts connecting the different parts. The dimensions in the current model are meant as illustrative suggestions.

The turbine should be design in such manner that it can be fitted to the existing penstock and draft tube outlet on Jhimruk power plant.

4.3 Sources of error

Boundary conditions

For the static structural analysis the runner is stationary with the pressure distribution from a rotating runner. I.e. forces like gravity and centrifugal force is neglected.

Mesh independence analysis

A mesh independence analysis was performed on one of the CFD analysis and one of the FEM analysis. Even though the remaining analyses were given similar meshes there is no guaranty that the mesh does not affect the solution of these analyses. This should be taken in to account if the results from this thesis are to be used in later work.

The mesh for the static structural analysis was not proven independent.

Chapter 5

Conclusion and further work

5.1 Conclusion

FSI analyses were performed on three different blade designs at best point operation. All the analyses showed stress well within the accepted limits. For the reference design the thickness was reduced and analysed at best point and full load. The stress for these analyses were also well within the limits. Thinner blades should be considered for further designs.

5.2 Further work

The following aspects should be considered for further work on this thesis:

- A grid independent mesh for the static structural analysis should be obtained.

- A new design for the hub should be modelled. The shaft connection should fit the current shaft arrangement on Jhimruk hydropower plant.

- A non-stationary FSI analysis should be performed on the runner.

- FSI analysis should be performed on thinner blades if the non-stationary analysis gives acceptable results for the current designs.

- Strength calculations and dimensioning of all bolts and connections should be performed.

- A welded design for the spiral casing and draft tube should be modelled.

- Proper hydraulic design should be found for the guide vanes and stay vanes and included in the model.

- FEM analyses should be performed on the following parts of the turbine model; Spiral casing, stay ring and draft tube.

Bibliography

[1] Hari P. Neopane. *Sediment erosion in hydro turbines*. PhD thesis, NTNU, March 2010.

[2] Bhola Thapa and Ole G. Dalhaug. Development of Francis turbine manufacturing and testing facility in Nepal(Project pre-proposal). June 2011.

[3] Mette Eltvik. Numerical analysis on effect of design parameters and sediment erosion on a Francis runner. 2012.

[4] Bhola Thapa. *Sand erosion in hydraulic machinery*. PhD thesis, NTNU, Waterpower laboratory, 2004.

[5] Jonas Bergmann-Paulsen. *Mechanical design of Francis turbine exposed to sediment erosion*. Waterpower laboratory, NTNU, 2011.

[6] Ola Gjølme Thorvaldsen. *Styrkeberegning av løpehjul i Francis turbiner*. Waterpower laboratory, NTNU, 2011.

[7] Helene P. Erichsen. Mechanical design of Francis turbine exposed to sediment erosion. Master's thesis, NTNU, Waterpower laboratory, June 2011.

[8] Kristine Gjøsæter. Hydraulic design of Francis turbine exposed to sediment erosion. Master's thesis, NTNU, Waterpower laboratory, June .

[9] Peter J. Gogstad. Hydraulic design of Francis turbine exposed to sediment erosion. Master's thesis, NTNU, Waterpower laboratory, June .

[10] Hermod Brekke. Konstruksjon av pumper og turbiner. Waterpower laboratory, NTNU, December 2008.

[11] Mei Zu-yan. *Mechanical design and manufacturing of hydraulic machinery*. International Editorial Committee, 1991.

[12] Ole G. Dahlhaug. Lecture notes in Turbomachinery. 2010.

[13] Arne Kjølle. Mechanical equipment. Waterpower laboratory, NTNU, June 2001.

[14] Kværner Energy. Hydro power Part 3: Turbines. August 1987.

[15] Professor Ole G. Dahlhaug. NTNU. Personal conversations. 2012.

[16] Kristine Gjøsæter. *Hydraulic design of Francis turbine exposed to sediment erosion*. Project thesis, NTNU, Waterpower laboratory, December 2010.

[17] Casper Vogt-Svendsen. *Mechanical design and manufacturing of hydraulic machinery*. International Editorial Committee, 1991.

[18] Prof emeritus Hermod Brekke. NTNU. Personal conversations. October 2011.

[19] Hermod Brekke. Hydraulic turbines - Design, erection and opperation. Waterpower labora-tory, NTNU, June 2001.

[20] Hermod Brekke. Pumper & Turbiner. Waterpower laboratory, NTNU, 2003.

[21] Zhao Wei, Pål Henrik Finstad, Grunde Olimstad, Eve Walseth, and Mette Eltvik. *High pressure hydraulic machinery*. Waterpower laboratory, NTNU.

[22] IEC 62364 Ed. 1.0 Hydraulic machines - Guide for dealing with abrasive erosion in water (CD/Draft). Technical report, 2011.

[23] Mette Eltvik. Sediment Erosion in Francis turbines. Master's thesis, NTNU, Waterpower laboratory, June 2009.

[24] ANSYS. ANSYS 14 - Help. 2012.

[25] Gouri Dhatt and Gilbert Touzot. *The Finite Element Method Displayed*. John Wiley & Sons, 1984.

[26] W Malaseka and H K Verseeg. *An introduction to Computational Fuid Dynamics - The finite volume method*. 2007.

[27] ANSYS. ANSYS Meshing User's Guide. November 2010.

[28] EDR ANSYS support. Personal conversations. 2012.

Appendix A

Drawing a section of the runner in Pro/Engineer

The model for the FEM-analysis of the runner is 1/17 part of the entire runner. A step by step method to create the section is described below. This model will be imported to ANSYS and requires fine tolerances. Make sure that all the angular tolerances is at maximum accuracy.

A.1 Blade

1. Import the following curve files from Khoj; centrelines.ibl, bladeps.ibl, bladess.ibl, hub.ibl and shroud.ibl. Figure A.1.1 shows the imported curves.

2. Use boundary blend between the curves from bladeps.ibl to make a quilt at the pressure side, repeat for the suction side.

3. Create a new datum plane through the corners of the two quilts at the leading edge. Sketch a line for the leading edge in the new datum plane.

4. Select the edge on the suction side quilt closest to the inlet. Use the function *Extend* and remove $3 \cdot r$. Repeat for the pressure side, remove $1 \cdot r$.

5. Create the leading edge by using *Boundary blend* between the two edges and the leading edge sketch. Select *Constraints* and set *Condition* to *Tangent*. Figure A.1.2 shows how shows the boundary blend between the edges and the sketch.

6. Use *Boundary blend* between the edges of the pressure- and suction side at the trailing edge.
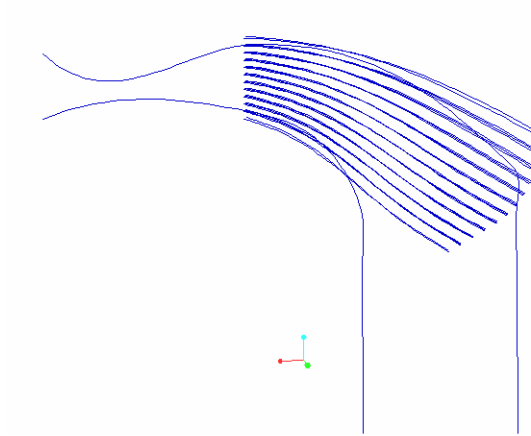
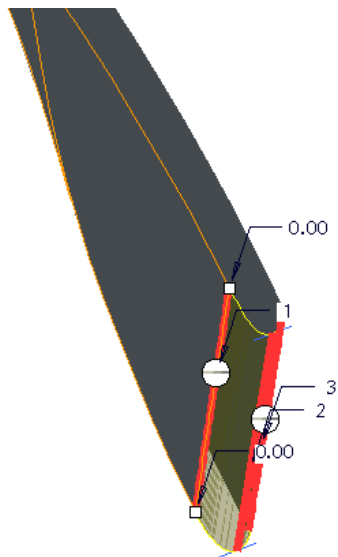Figure A.1.1: Imported curves in Pro/engineer

Figure A.1.2: using boundary blend to create the leading edge

7. Select the suction side edge and use *Extend* to remove $\frac{2}{3} \cdot thickness$ towards the suction side. select the new edge on the suction side quilt and remove $\frac{2}{3 \cdot \tan 30} \cdot thickness$ by using *Extend*. Use *Boundary blend* to close the gap at the trailing edge, figure A.1.3 this step.
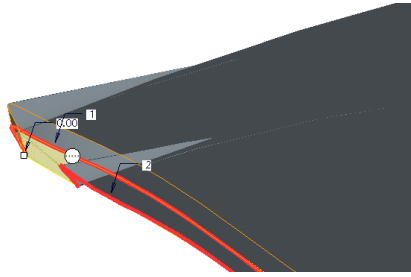
8. Use *Merge* on the 5 quilts.

Figure A.1.3: Using boundary blend to create the trailing edge

9. Start a sketch in the *Top* plane. Select *Use edge* on the hub curve. Revolve the sketch around the z-axis.

10. it Merge the blade and the revolved hub sketch so that only the blade remains. Repeat the steps for the shroud line. Figure A.1.4 shows this step.
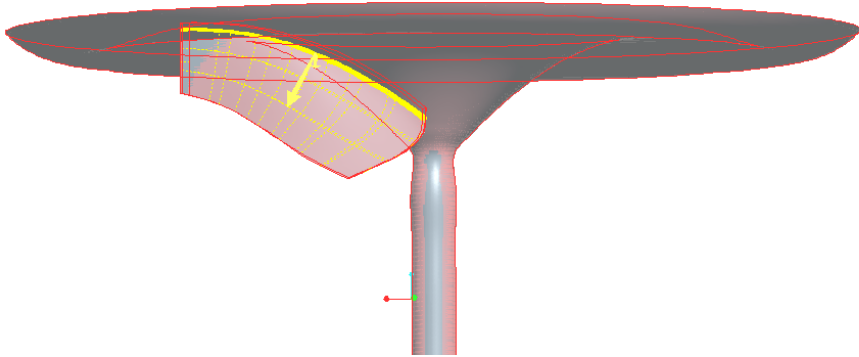

Figure A.1.4: Merging the blade and the hub quilt

11. Use it Solidify on the blade.

A.2   Hub and shroud

If there already exist a hub and shroud geometry the next steps can be simplified by publishing the geometries and importing it in to the current part.

1. Start a sketch in the *Top*-plane. If a hub geometry already exist, import it and select *Use edge* to copy it into the sketch. If not, select *Use edge* on the hub-curve and draw a geometry for the hub.

2. Revolve the sketch as a surface, select *Revolve on both sides*. Do not revolve it 360 degrees, make sure there is a small section where the ends does not connect.

3. Create a new datum plane parallel to the *Front*-plane with a big offset (ex. 500 mm) and. Repeat in the opposite direction.

4. Start a sketch in the one of the new planes. Select *use edge* on the upper curve from the center lines. Draw a tangent line from the leading edge so it goes past the hub. Draw a circular section from the trailing edge to the center of the turbine, place the center of the circular section so that the end is tangent to the curve. Select all the lines and use *Move and resize* select the *Rotate/Scale* reference to be the center of the turbine. Rotate $\frac{360}{2\cdot17}$. This should be calculated outside pro engineer and imported since the accuracy in Pro/engineer calculations only support an two decimals.

5. Use the function *Project*. Project the sketch to the other new datum plane.

6. use *Boundary blend* between the new sketch and the projection. Figure A.2.1 shows the hub shell with a quilt going from the sketch to the projection.

7. Merge the revolved hub and the quilt.

8. Make an axial pattern of the quilt with an angular offset of $\frac{360}{17}$. Again, do not make the calculation directly in Pro/Engineer as this will result in coarse accuracy due to round off.

9. Merge the patterned quilt with the hub.

10. Use *Solidify* on the hub shell.

11. Repeat the procedure for the shroud. Figure A.2.2 shows the finished section.
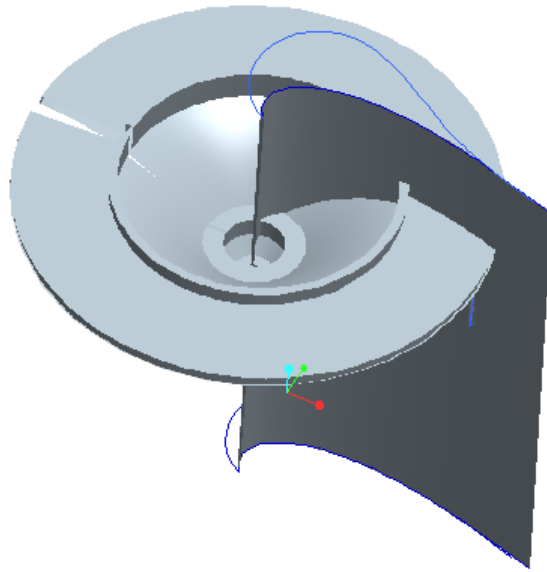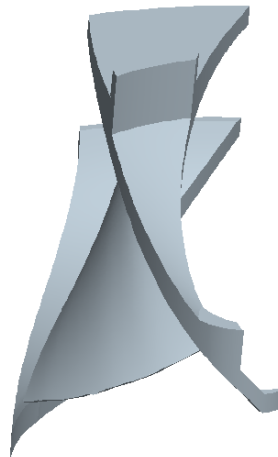
Figure A.2.1: Hub with quilt defining the border of the section

Figure A.2.2: Finished section